

# 110 W(0.9 J) pulsed power from resonantly diode-laser-pumped 1.6- $\mu\text{m}$ Er:YAG laser

Dmitri Garbuzov<sup>a)</sup> and Igor Kudryashov

Princeton Lightwave Inc., 2555 US Route 130, Cranbury, New Jersey 08512

Mark Dubinskii

U.S. Army Research Laboratory, AMSRD-ARL-SE-EO, 2800 Powder Mill Road, Adelphi, Maryland 20783

(Received 25 April 2005; accepted 27 July 2005; published online 12 September 2005)

110 W pulse power and 0.93 J pulse energy have been obtained with direct resonant pumping of a 1.6- $\mu\text{m}$  Er<sup>3+</sup>-doped bulk solid-state laser with two-dimensional stacks of 1.5  $\mu\text{m}$  InGaAsP/InP diode lasers. © 2005 American Institute of Physics. [DOI: 10.1063/1.2051803]

Diode-pumped Yb:YAG solid-state lasers (DP SSL) resonantly pumped by GaAs-diode lasers and operating in a quasi-three-level scheme demonstrate superior performance among solid-state sources of coherent radiation.<sup>1</sup> The resonance pumping approach can also be used for Er<sup>3+</sup>:YAG SSLs operating in the eye-safe 1.6- $\mu\text{m}$  spectral range. Based on considerations of atmospheric transparency and eye safety, fiber lasers of this spectral range are widely used for long-distance telemetry and ranging. However, for high-energy laser applications an optical damage threshold higher than that of glass, and much better thermal conductivity of the gain medium, drive the interest toward bulk solid-state lasers operating in the same spectral range.<sup>2</sup>

Last year, 54% optical-to-optical slope efficiency was obtained for a 1.6- $\mu\text{m}$  Er:YAG SSL resonantly pumped with a 1532-nm fiber laser.<sup>3</sup> This year, we demonstrated 26% photon-to-absorbed photon efficiency for a low-power Er (1%):YAG SSL resonantly pumped by a single-mode InGaAsP/InP diode laser.<sup>4</sup>

An extremely low photon defect (5.3%) realized with 1530 nm pumping is one of the attractive features of the development of DP SSLs with InGaAsP/InP-based pumping systems. Another advantage of the InGaAsP/InP-based pumping systems is their superior manufacturability and operational lifetime. InGaAsP/InP-based diode lasers do not require the sophisticated mirror facet coating needed for high-power GaAs-based emitters. The technology used in the fabrication of these lasers is well developed since it originated in the telecom industry where 10<sup>6</sup> h of operational lifetime are required for single-mode InGaAsP/InP emitters. We also demonstrated operational lifetimes approaching 10<sup>6</sup> h for multimode high-power InP-based diode laser arrays.<sup>5</sup>

Reported in this paper are the results of the direct resonant pumping of a 1.6- $\mu\text{m}$  Er(0.5%):YAG SSL with two-dimensional stacks of 1470 and 1530 nm InGaAsP/InP diode lasers. The 0.5% Er doping level was selected based on the results of our previous studies, where we found that for DP SSL with a 1% YAG doping level the threshold is increased threefold due to up conversion.<sup>4</sup> Diode laser stacks of 1470 nm were fabricated using a design platform based on a quantum well separated confinement laser structure with a narrow waveguide.<sup>5</sup> A 1530-nm stack was composed of arrays fabricated from a quantum well structure with a broad

waveguide.<sup>6</sup> Fast axis full width at half maximum (FWHM) divergences for 1470 and 1530 nm emitters are 30° and 42°, respectively. Broad waveguide 1530 nm laser stacks have a lower threshold and higher differential efficiency than that for narrow waveguide emitters (Fig. 1). Power-current characteristics of Fig. 1 were recorded in CW up to 100 A. The data of Fig. 1 refer to the stacks of 10 diode laser arrays mounted on microchannel coolers and assembled with a 1.8-mm pitch between arrays. Each array consists of 19 emitters with apertures of 100  $\mu\text{m}$ . In pumping experiments, at a 1 Hz repetition rate these diode laser stacks operated up to 180 A.

In the experiments described here, a 4-cm-long, 3.5-mm-diam, Er<sup>3+</sup>(0.5%):YAG laser rod was single-end pumped in a straight cavity as shown in Fig. 2. The rod had an antireflective coating with  $R < 0.2\%$  at both facets and an unpolished barrel. The rod was placed in a gold-plated cylindrical reflector with a diameter of 3.7 mm and composed of a half-cylindrical base and cover parts. No thermoconductive materials were used in the gap between the rod and the reflector. Because of the absence of heat sinking, the measurements were performed at a repetition rate as low as 1 Hz. Pumping pulses with durations of 5 and 10 ms were used. The pulse duration is limited by the upper laser level lifetime (7 ms) on the short side and by rod heating on the long side. The SSL operates at 1645 nm wavelength. The shapes of the pumping pulse and the SSL output pulse were measured using a Ge photodetector. The SSL output pulse is shorter than the pumping pulse by the turn-on time, which decreases from 3 ms near threshold to 0.8 ms at maximum power.

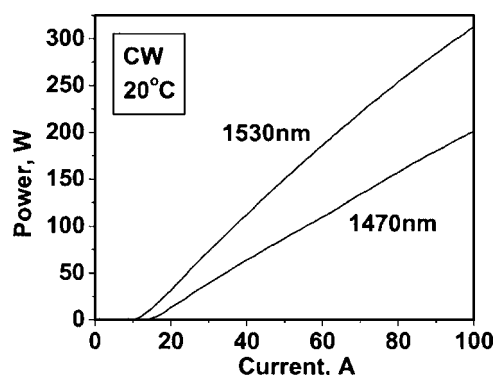


FIG. 1. CW power-current characteristics of 1530 and 1470 nm, ten-array, diode laser stacks.

<sup>a)</sup>Electronic mail: dgarbuzov@princetonlightwave.com

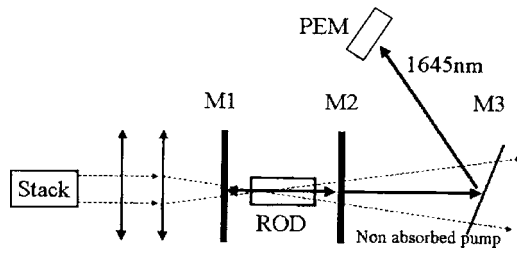


FIG. 2. Optical layout of DP SSL. (*M1*) and (*M2*) plano-plano dichroic mirror and output coupler; (*M3*) second dichroic mirror; (*PEM*) pulse energy meter.

Pumping radiation from a diode laser stack after collimation was coupled into the rod end through a dichroic plano-plano mirror *M1*. On one side, mirror *M1* had an antireflective coating for pumping radiation. The coating on the other side of the mirror provided a transparency of greater than 95% for pumping radiation and higher than 99.8% reflection for SSL radiation in the wavelength range of 1605–1670 nm. The highest SSL output powers were obtained using a flat output coupler with a transparency of 13.9%.

The results of beam tracing in the rod without absorption for the pumping beam are shown in Fig. 3. The incident diameter of the pumping beam after shaping optics was less than the rod diameter, and more than 99% of the pump radiation was coupled into the rod. A beam waist with a diameter of about 2 mm was located in the first half of the rod facing the pump radiation. Due to beam divergence, the pumped rod volume is larger in the second half of the rod, and about 30% of the radiation not absorbed in the first half of the rod can be scattered by the unpolished rod barrel surface. For some portion of this radiation, additional nonactive losses are possible due to less than 100% reflection at the plated reflector surface. These losses were not accounted for when absorbed power (energy) was calculated (Fig. 4). In these calculations, the upper limit of absorbed power was calculated as a difference between the incident pumping power and postrod pumping power. A pulse energy meter (*PEM*) was used for the pumping and output SSL power measurements. For measurements of the postrod pumping power, a *PEM* head of 3.3 cm diam was positioned 5 mm from the rod end. For SSL output power measurements, the second highly reflective dichroic mirror (*M3*) was used to eliminate the contribution of nonabsorbed pumping radiation (Fig. 2). The energy readings from the *PEM* and SSL pulse duration FWHM values were used to calculate and then plot the powers in Fig. 4 (bottom and left axis).

In order to achieve the maximum SSL output powers, the pumping spectrum should be located at the optimum position

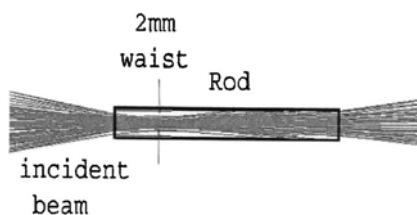


FIG. 3. Ray tracing result for stack pumping beam shaped by collimating optics. It was assumed that the barrel surface is 100% absorptive to establish that at least 70% of the incident rays can propagate without interacting with the rod barrel.

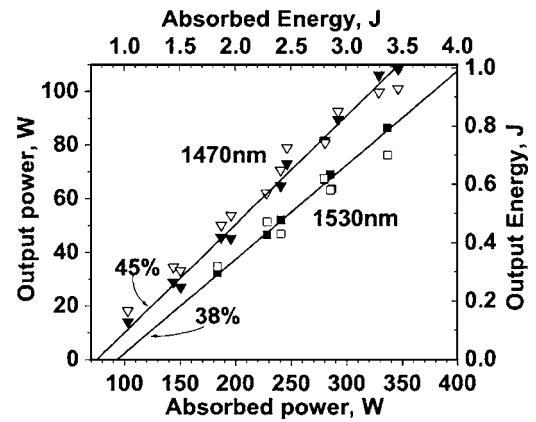


FIG. 4. Output characteristics of DP SSL pumped at 1470 nm (triangles) and 1530 nm (squares). The open and solids symbols refer to power in 5 ms pulses (bottom and left axes) and energy in 10 ms (top and right axes).

relative to the system of absorption  $\text{Er}^{3+}$  lines. Examples of such optimized spectrum positions for 1470 and 1530 nm pumps are given in Figs. 5 and 6. The postrod spectra measured at 80 A stack currents and 16 °C water temperature are shown as the envelopes of the shaded areas in these figures. To keep the optimum position of the pumping spectra at higher pumping powers, the water temperature was decreased as indicated on the other two spectra shown in Figs. 5 and 6. For each of the three indicated water temperatures, three to four data points were taken to plot the optical-to-optical characteristics of Fig. 4. The water temperature adjustment allows us to keep the temperature of the array active regions almost constant throughout the whole range of pumping powers. At these conditions, only a 2–3 nm increase in the pumping spectrum FWHM with current increase was observed (Figs. 5 and 6). The portion of absorbed power was almost independent of current and equal to 80% and 70% for 1470 and 1530 nm pumps, respectively.

The photon-to-absorbed photon efficiencies calculated from the slopes of the optical-to-optical characteristics are 45% and 38% for 1470 and 1530 nm pumps, respectively. The maximum powers are 110 and 85 W for 5 ms pulses of 1470 and 1530 nm pump radiation (solid triangles and squares, bottom and left scales of Fig. 4). Energies of 0.93 J(1470 nm) and 0.7 J(1530 nm) have been achieved

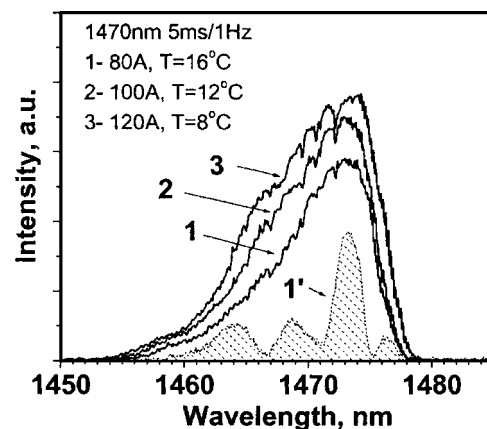


FIG. 5. 1, 2, and 3—1470 nm stack spectra measured at currents 80, 100, and 120 A (5 ms pulses); 1'—Postrod spectrum at 80 A pumping. The shaded area is proportional to the nonabsorbed portions of the spectrum shown by curve 1.

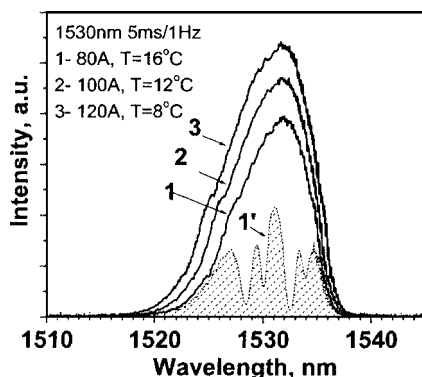


FIG. 6. 1, 2, and 3—1530 nm stack spectra measured at currents 80, 100, and 120 A (5 ms pulses); 1'—Postrod spectrum at 80 A pumping. The shaded area is proportional to the nonabsorbed portions of the spectrum shown by curve 1.

with 10 ms pumping pulses (open triangles and squares, top and right scales of Fig. 4). We believe that the higher power and efficiency of 1470 nm pumps compared with 1530 nm pumps observed in these experiments could be associated with the higher absorption for the 1470-nm line group. High absorption increases the portion of the pumping photons absorbed in the first half of the rod where the waist of the pumping beam is located. As a result, a pumping coefficient ( $\eta_p$ ) that is proportional to the ratio of lasing mode and pumping volumes in the rod could be higher for the 1470-nm pumping than for the 1530-nm pumping.

In order to establish the factors limiting the slope efficiency we measured the optical-to-optical characteristics for DP SSL with different output coupler transmissions ( $T$ ) and estimated the beam diameter in the rod using an InGaAs snapshot camera. We found that the diameter of the lasing beam waist is about 1 mm while the slope efficiency is al-

most independent of  $T$  in the range  $10\% < T < 25\%$ . These results allow us to conclude that the DP SSL obtained slope efficiency (46%) is determined by the value of  $\eta_p$  rather than the value of the optical intracavity losses.

We reported the effective direct resonant pumping of a 1.6- $\mu\text{m}$   $\text{Er}^{3+}$ :YAG SSL using two-dimensional stacks of 1470 and 1530 nm InGaAsP/InP diode lasers as the pump sources. A 4-cm-long, 3.5-mm-diam,  $\text{Er}^{3+}$ (0.5%):YAG laser rod was single-end pumped in a straight cavity. The rod did not have a heat sink, and the SSL operates with a 1-Hz repetition rate. In the case of 1470 nm diode laser pumping the photon-to-absorbed photon efficiency was as high as 46%, the maximum power was 110 W at 5 ms pumping pulses, and the maximum energy was 0.93 J at 10 ms pumping pulses. With a 1530-nm pump, the same parameters were 38%, 85 W, and 0.7 J. We believe that the achieved powers and energy are a record high for diode-pumped SSL operating in the eye-safe wavelength range. For example, for a 1.6- $\mu\text{m}$   $\text{Er}^{3+}$ :YAG SSL with a GaAs-based pump system the record pulse energy is 0.08 J (Ref. 2).

This work was supported by the HEL-JTO/AF through the BAA under Contract No. FA9451-04-C-0189. The authors acknowledge M. Itzler for creative discussions.

<sup>1</sup>W. F. Krupke, IEEE J. Sel. Top. Quantum Electron. **6**, 1287 (2000).

<sup>2</sup>E. Georgiou, F. Kiriakidi, O. Musset, and J. Boquillon, Proc. SPIE **5460**, 272 (2004).

<sup>3</sup>Y. Young, S. Setzler, K. Snell, P. Budni, T. Pollak, and E. Chicklis, Opt. Lett. **29**, 1075 (2004).

<sup>4</sup>D. Garbuzov, I. Kudryashov, and M. Dubinskii, Appl. Phys. Lett. **86**, 1 (2005).

<sup>5</sup>D. Garbuzov, I. Kudryashov, and A. Komissarov, Proc. SPIE Int. Soc. Opt. Eng. **5594**, 124 (2004).

<sup>6</sup>D. Garbuzov, L. Xu, S. R. Forrest, R. Menna, R. Martinelli, and J. C. Connolly, Electron. Lett. **32**, 1717 (1996).